A Novel Six-band Dual CP Rectenna Using Improved Impedance Matching Technique for Ambient RF Energy Harvesting

Chaoyun Song, *Student Member*, Yi Huang, *Senior Member*, *IEEE*, Paul Carter, Jiafeng Zhou, Sheng Yuan, Qian Xu and Muayad Kod

***Abstract*— A novel six-band dual circular polarization (CP) rectenna for ambient RF energy harvesting is presented. Due to the non-linearity and the complex input impedance of the rectifying circuit, the design of a multiband and/or broadband rectenna is always challenging and the performance of rectenna can be easily affected by the variation in such as the input power level and load. Therefore, an improved impedance matching technique is introduced which is aimed to improve the performance of the rectifier with a varying condition. A broadband dual CP receiving antenna is proposed which has a very wide bandwidth (from 550 MHz to 2.5 GHz) and a compact size. An annular ring structure and a novel feeding technique are employed in order to reduce the size and improve the antenna performance. As a result, the proposed rectenna is the first design which covers six frequency bands, including part of the Digital TV and most of the cellular mobile and WLAN bands in the U.K., while the optimal load range for a constant conversion efficiency is from 10 kΩ to 75 kΩ. The measured results show that the maximum harvested DC power of the rectenna in typical outdoor and indoor environments are 26 μW and 8 μW respectively; it can therefore be applied to a range of low power wireless applications.**

***Index Terms*—Broadband dual CP antenna, rectifier, broadband rectifier, RF energy harvesting.**

I. Introduction

SELF-SUSTAINABLE low power electronic devices for applications such as the Internet of Things (IoT), smart cities, and wireless sensor networks have attracted significant attention in the past few years. There is an increasing demand for energy harvesting technologies with the aim to replace the battery and save maintenance cost. Radio-frequency (RF) energy harvesting from the ambient electromagnetic (EM) waves is one of the most favorable technologies for supplying continuous power to these standalone devices [1]. The concept of RF energy harvesting was raised in the early 1990s while rectifying antenna (rectenna) technology has been employed to convert microwave power to DC power much earlier [2].

Generally, a rectenna consists of a receiving antenna and a rectifying circuit. The overall RF-to-DC conversion efficiency is the most vital parameter to evaluate the performance of a rectenna. Some rectennas have achieved very high conversion efficiency (e.g. >80%) [3]–[6]. However, these designs were mainly for a single narrow frequency band and required a relatively high input power level (such as 10 dBm [3], 0 dBm [4], 13 dBm [5], and 6 dBm [6]) which is not appropriate for ambient RF energy harvesting. Ambient EM signals are normally available at low levels and distributed in multiple frequency bands. Some designs combine the output DC powers from different single band rectennas [31], but the overall conversion efficiency was low and still limited by the intrinsic power consumption of the rectenna. Thus, the design of a multiband or broadband rectenna which can harvest ambient RF energy from different frequency bands simultaneously is of great importance. Due to the non-linearity of the rectifier, the input impedance of the circuit is varies as a function of frequency, input power level and also load impedance. Thus the multiband or broadband design is very challenging. Some dual-band rectennas, multiband rectennas, and broadband rectennas have been proposed [7]–[13] but there are various limitations.

In some applications, the output of a rectenna is directly connected to a device such as a DC-to-DC converter, a power management unit (PMU) or a super capacitor in order to manage and store the DC power properly. In these cases, the load of the rectenna is time-varying which results in the variation of the input impedance of the rectifier [15], [16]. For the conventional rectenna design with a fixed load resistance, the overall conversion efficiency over the broadband is low due to the impedance mismatch. To solve this problem, some approaches (such as the resistance compression network, and the resistance controlled DC-DC converter to keep the conversion efficiency stable in a wide range of load) have been reported in [14]–[20].

Since the ambient EM waves are normally of arbitrary polarization and random incident angles, the antenna for RF energy harvesting should be of omnidirectional radiation pattern and wide operational frequency band. Some antennas such as the microstrip patch [3], dipole [9], spiral [11], loop [4], and cross dipole [13] for energy harvesting application have

Manuscript received November 2, 2015; revised January 25, 2016; accepted May 1, 2016. This work was supported in part by the EPSRC (UK) and in part by the Aeternum LLC.

C. Song, Y. Huang, J. Zhou, S. Yuan, Q. Xu, and M. Kod are with the Department of Electrical Engineering and Electronics, The University of Liverpool, Liverpool L69 3GJ, U.K. (e-mail: sgcsong2@liv.ac.uk; yi.huang@liv.ac.uk).

P. Carter is with Global Wireless Solutions, Inc., Dulles, VA 20166, USA.

been proposed in the literature. Wideband dual linear polarization (LP) or CP antennas have achieved the best performance.

Most reported rectennas are optimized to a fixed load but very few designs can produce a constant conversion efficiency with a varying load as we used in practice. In addition, so far no published designs can harvest energy from the DTV (Digital TV), cellular mobile and WiFi bands (from 470 MHz to 2.5 GHz) simultaneously. Thus in this paper, we propose a novel rectenna using an improved impedance matching technique. First of all, the characteristics of the non-linearity of the rectifier are studied. The novel matching network is then designed and optimized to match the impedance at six frequency bands which cover the U.K. DTV channel 30-37 (550 – 600 MHz), 55-62 and LTE/4G (750 – 800 MHz), GSM900 (850 – 910 MHz), GSM1800/4G (1850 – 1900 MHz), UMTS/3G (2150 – 2200 MHz), and WiFi (2400 – 2450 MHz) at the ambient input power levels which are typically from -30 dBm to -5 dBm. An additional section is added to the matching network in order to maintain the good performance of the rectifier with a wide range of load, from 10 kΩ to 75 kΩ (which are the typical values for many sensors). A broadband dual linear polarization (LP) cross dipole is modified as a frequency-independent dual CP cross dipole by introducing a self-complementary log-periodic structure and a novel feeding structure. In addition, an annular ring is used to reduce the antenna size. The simulated maximum conversion efficiency of the rectenna at a single frequency is about 67% with -5 dBm input power. To the best of our knowledge, the proposed rectenna is the first design which covers a wide frequency and load impedance range with a relatively constant high conversion efficiency.

The rest of this paper is organized as follows. Section II introduces non-linear analysis of the rectifier circuit and details about the improved impedance matching technique. A broadband dual CP receiving antenna design is discussed in Section III. The experimental results of the rectenna including indoor and outdoor measurements are presented in Section IV. Finally, conclusions are drawn in Section V.

II. SIX-BAND NOVEL RECTIFIER DESIGN

A. Non-linear Analysis of the Rectifier Input Impedance

There have been various types of rectifier topologies such as single series diode rectifiers, single shunt diode rectifiers, voltage doubler rectifiers, and bright type rectifiers. Comprehensive comparisons of different rectifier circuits have been made in [21] and [22]. The single-stage standard full-wave voltage doubler rectifier is a good choice for RF energy harvesting, since it has a higher efficiency and output power compared to a single series half-wave rectifier. In addition, it can minimize the extra losses introduced by multi-stage rectifiers, which is significant at low power levels. The configuration of a voltage doubler rectifier is depicted in Fig.1. Let a sinusoidal signal input to the rectifier which can be expressed as $v_{in} = V_{AC} \sin \omega t$, where V_{AC} is the amplitude and ω is the frequency of the input signal. The negative half cycle of

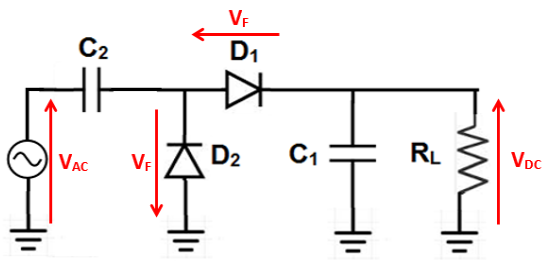

Fig. 1. Configuration of a voltage doubler rectifier circuit.

the wave is rectified by the shunt diode D_2 and the energy is stored in C_2. The positive half cycle is rectified by the series diode D_1 and the energy is store in C_1. During the next period, the energy in C_2 is transferred to C_1 and then discharged to the load resistor R_L. Thus the output DC voltage can be calculated by.

$$V_{DC} = 2V_{AC} \sin \omega t - 2V_F \quad (1)$$

where V_{DC} is the output voltage and V_F is the forward bias voltage of the diode. From the theory [12], the instantaneous current flow through the diode expressed in terms of the time varying input is shown in (2), where I_S is the saturation current of the diode, V_T is the thermal voltage, and m is the ideality factor.

$$I_D = I_S \left[\exp\left(\frac{V_{AC} \sin \omega t - 0.5V_{DC}}{mV_T} \right) - 1 \right] \quad (2)$$

Using the modified Bessel function series expansion, similarly to [15], as given in (3)

$$\exp(x \cos \omega t) = B_0(x) + 2 \sum_{n=1}^{\infty} B_n(x) \cos(n\omega t) \quad (3)$$

The current through the diode I_D can be expressed as the sum of the DC component and the harmonic contributions as shown in (4). The DC part of the current I_{DC} is then extracted as in (5).

$$I_D = I_S \left[B_0\left(\frac{V_{AC}}{mV_T}\right) \exp\left(\frac{-0.5V_{DC}}{mV_T}\right) - 1 \right] + 2I_S \sum_{n=1}^{\infty} B_n\left(\frac{V_{AC}}{mV_T}\right) \exp\left(\frac{-0.5V_{DC}}{mV_T}\right) \cos\left(\frac{n\pi}{2} + n\omega t\right) \quad (4)$$

$$I_{DC} = I_S \left[B_0\left(\frac{V_{AC}}{mV_T}\right) \exp\left(\frac{-0.5V_{DC}}{mV_T}\right) - 1 \right] \quad (5)$$

Since the equivalent impedance of the diode equals to the voltage difference across the diode terminals (V_F) divided by the current flow into the diode from (5), the input impedance of the diode can be expressed as

$$Z_{diode} = \frac{V_F}{I_{DC}} = \frac{V_{AC} \sin \omega t - 0.5V_{DC}}{I_S \left[B_0\left(\frac{V_{AC}}{mV_T}\right) exp\left(\frac{-0.5V_{DC}}{mV_T}\right) - 1 \right]} \quad (6)$$

Thus, as shown in (6), the input impedance of the diode depends on the input power level (V_{AC}) as well as the angular

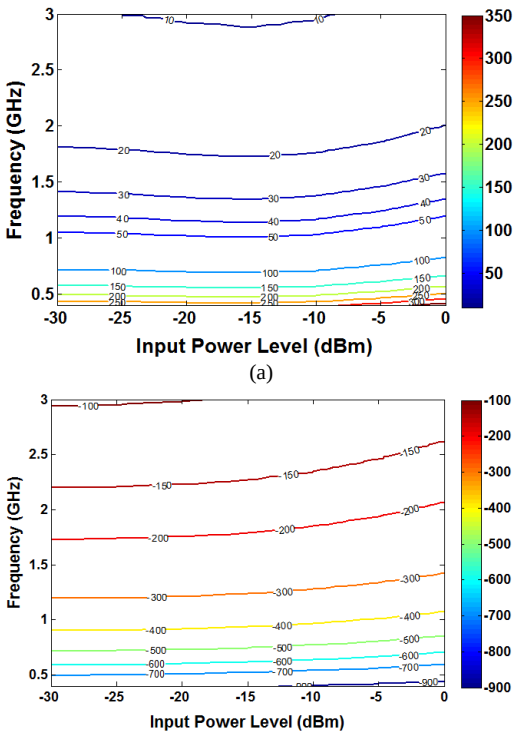

Fig. 2. The input impedance of the voltage doubler rectifier versus frequency and input power level for the load resistance of 25 kΩ. (a) Real part. (b) Imaginary part.

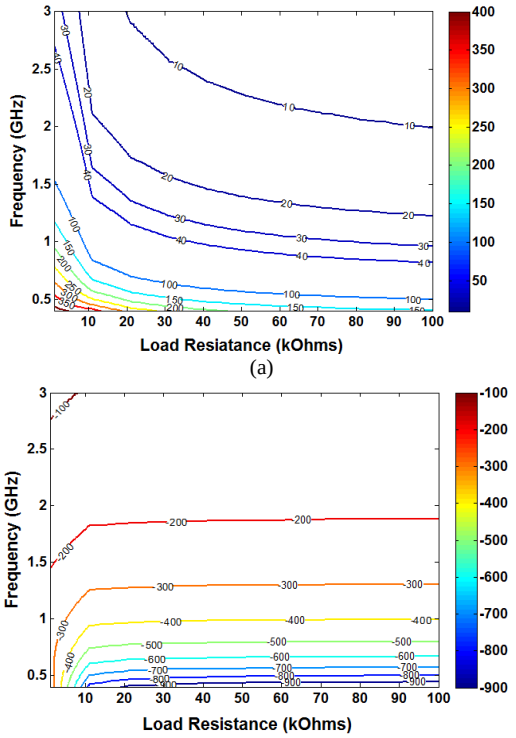

Fig. 3. The input impedance of the voltage doubler rectifier versus frequency and load resistance with the input power level at -30 dBm. (a) Real part. (b) Imaginary part.

frequency (ω). In addition, since the output voltage can be calculated by $V_{DC} = I_{DC} \times R_L$, where I_{DC} is the output DC current and R_L is the load resistance, the input impedance of the diode is also strongly influenced by the value of the load.

In order to gain a better understanding of the non-linear input impedance of the voltage doubler rectifier, a circuit was designed and analyzed by using the large signal S-parameter (LSSP) simulation using ADS software. The diode selected is a Schottky diode SMS7630 due to its low forward bias voltage and high saturation current. A non-linear spice model with parasitic elements, provided by Skyworks Solution Inc. [23], was used in the simulation. The value of the selected capacitors is 100 nF which is a typical value for this application and the value of the capacitors will not affect the input impedance of the rectifier. The function of the capacitor is to store the energy and smooth the output DC waveform. The simulated input impedance of the voltage doubler rectifier, including the real part and imaginary part, are depicted in Figs. 2(a) and (b) as a function of the frequency and the input power level respectively. The input impedance as a function of the frequency and the load are also shown in Figs. 3(a) and (b).

It can be seen that the real part of the input impedance changes significantly (from 10 to 300 Ω) against the frequency when the input power level is high (e.g. > -5 dBm), and load resistance is small (e.g. < 15 kΩ). The imaginary part of the impedance is not very sensitive to the variations of the input power level and the load resistance, but it changes rapidly from -100 (at 3 GHz) to -700 (at 0.55 GHz) which posts challenges in matching network design.

B. *Improved Impedance Matching Technique*

The impedance matching circuit is very crucial since it affects how much power can be delivered from the input to the junction of the diode. The conventional matching circuit for the rectifier is normally optimized for a fixed specific operating condition, including frequency, input power level and load impedance. From the analysis in Section II (A), it is noted that the conventional rectenna is not efficient for RF energy harvesting due to the varying operating conditions. Thus a novel impedance matching approach is proposed to improve the overall performance of the rectenna. The entire design process is explained as follows.

First of all, as a starting point, a dual-band bandpass impedance matching network is designed to match the input impedance of a single voltage doubler rectifier to a resistive port (50 Ω). To achieve the bandpass response and the dual-band impedance matching, the matching network should consist of a LC bandpass matching topology (4th order) at the first frequency and a modified L-network (2nd order) to cover the second frequency. Thus, the proposed matching network is a sixth-order lumped-element matching network. As shown in Fig. 4, the initial matching network consists of a shunt LC pair (L_1, C_1), a series LC pair (L_2, C_2), a shunt inductor (L_3) and a series inductor (L_4) which aims to get the rectifier matched at two frequency bands as well as a range of ambient input power level (-30 dBm to -5 dBm). Different from the conventional dual-band bandpass impedance matching network which normally consists of two shunt and series LC pairs (eighth-order) [15], the proposed matching network has

reduced the number of circuit elements and has a simpler topology. The non-linear input impedance of the voltage doubler rectifier, similar to Figs. 2 and 3, is exported to the touchstone S1P files. The Impedance Matching Toolkits in the ADS software is then employed to choose the values of the inductors and capacitors. The center frequencies are optimized at 550 MHz and 750 MHz while the desired bandwidth is set as 50 MHz at each band. In addition, the matching network is also optimized to have a bandpass response in order to reject higher order harmonics generated by the non-linear elements and improve the overall conversion efficiency.

Secondly, an additional section including a microstrip transmission line with a dimension of $W_{TL} \times L_{TL}$ and a shunt radial stub with width W, length L, and angle β is inserted between the inductors L_3 and L_4, as depicted in Fig. 5. The function of this additional section is to maintain the performance of the rectifier over a wide range of load values. The impedance mismatch caused by the variation of the load, as shown in Figs. 3(a) and (b), can be reduced by tuning the dimensions of the microstrip line at different loads. Thus, the LSSP and the Harmonic Balance (HB) simulation in ADS are employed to optimize the reflection coefficient S_{11} and conversion efficiency as a function of the load resistance from 1 kΩ to 100 kΩ. Note that the performance of the initial matching network should be maintained after adding this additional section. This can be achieved by setting additional goals during the optimization.

Thirdly, in order to design the matching network to cover six frequency bands, the initial dual-band matching network is used as a unit cell (Cell 1) and two additional cells (Cell 2 and Cell 3) are proposed accordingly. Cell 2 and Cell 3 are designed using the same approaches as introduced in the previous steps, but the center frequencies are modified to 900 MHz, 1.85 GHz, 2.15 GHz and 2.45 GHz respectively. As shown in Fig. 6, the three cells are distributed in three branches, each branch is connected to a single voltage doubler circuit as we have proposed in Section II (A). The three voltage doubler rectifiers are connected in series in order to obtain a higher output voltage. The input RF signal can only pass through the cell with the right frequency but will be rejected by the other cells. If one of the three branches is broken (open circuit), the other two cells can still work well. In addition, due to the non-linearity of the rectifier, the input impedance of the rectifier will be changed if we modify the circuit topology. Thus, the whole matching network including three unit cells is then re-optimized for the desired six center frequencies as well as the input power level and the load range.

The S_{11} and conversion efficiency of the proposed rectifier are optimized for a range of conditions such as different input power levels, multiple frequency bands, and a wide range of load. The non-linear effects on the input impedance have been fully considered thus the performance of the rectifier is maintained for various conditions. In order to improve the accuracy, the lumped elements were replaced by real product models including S-parameter files provided by the supplier such as Murata and Coilcraft. An EM simulation was conducted to analyze the dielectric loss of the substrate and insertion loss of the microstrip line. The optimized parameters after optimization are given in Table I. The final topology of the proposed rectifier is shown in Fig. 7 with a fabricated example. The substrate is Duriod 5880 with a relative permittivity of 2.2 and a thickness of 1.575 mm.

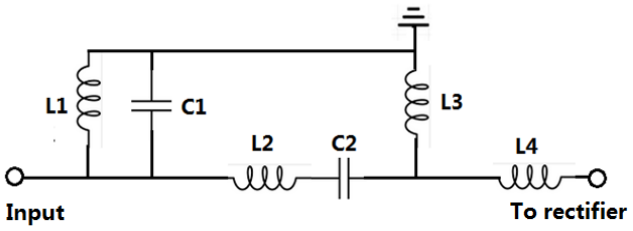

Fig. 4. The initial dual-band bandpass matching network with input power levels of interest from -30 to -5 dBm.

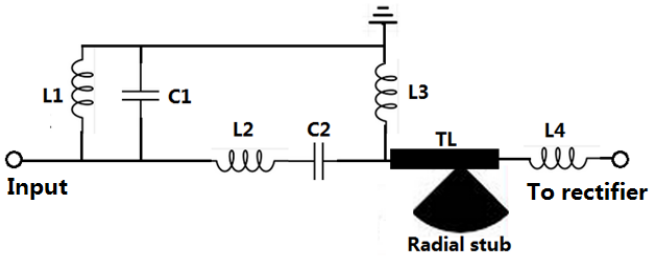

Fig. 5. The proposed matching network with performance maintained for a range of load impedance from 1 kΩ to 100 kΩ.

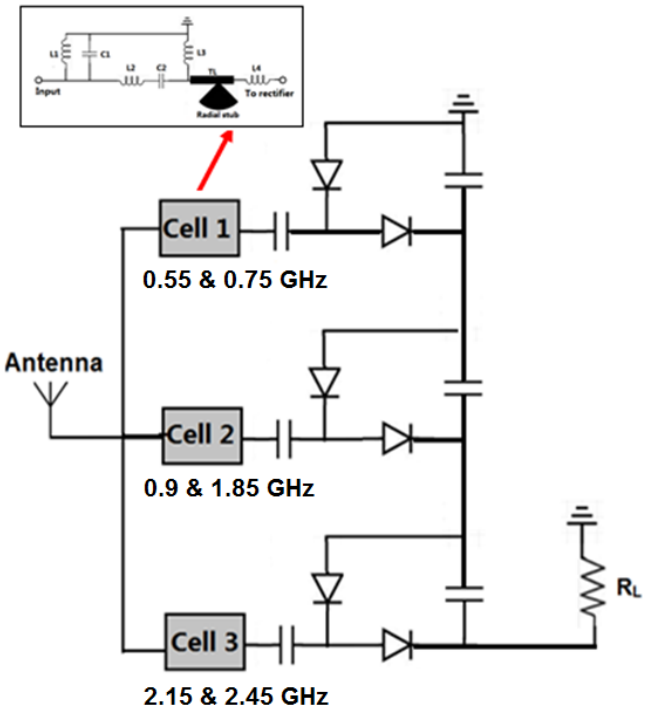

Fig. 6. The proposed six-band rectifier with an improved impedance matching network.

TABLE I
THE OPTIMIZED PARAMETERS OF THE PROPOSED RECTIFIER

Parameters	Cell 1	Cell 2	Cell 3
L1	9.87 nH	5.84 nH	21.31 nH
C1	2.5 pF	26.3 pF	3.9 pF
L2	3.18 nH	1.34 nH	52.18 nH
C2	4 pF	26.9 pF	2.3 pF
L3	12.43 nH	51.69 nH	17.33 nH
L4	20.49 nH	15 nH	13.74 nH
W_{TL}	1.5 mm	1.5 mm	1.5 mm
L_{TL}	4 mm	4 mm	1 mm
W	2 mm	1.3 mm	1.5 mm
L	5.93 mm	2.93 mm	4.48 mm
β	103°	106°	94°

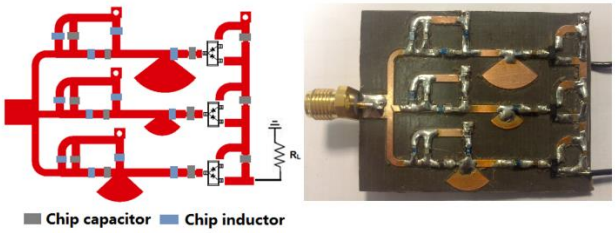

Fig. 7. Topology and fabricated prototype of the proposed six-band rectifier. The size of the PCB is 3.5 × 4.5 cm^2.

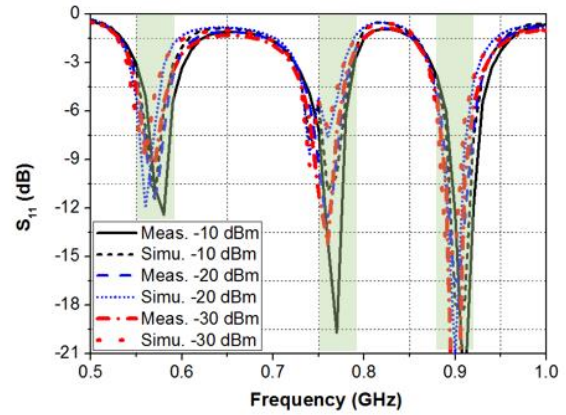

(a)

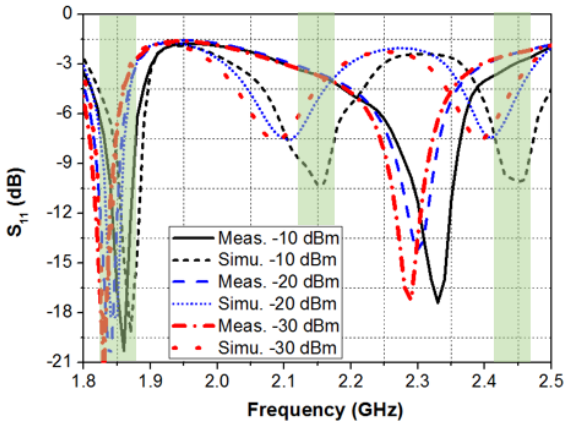

(b)

Fig. 8. The measured and simulated S_{11} of the proposed rectifier at three input power levels for the load resistance of 25 kΩ. (a) The lower three bands. (b) The higher three bands.

C. *Rectifier Performance*

The simulated and measured reflection coefficients of the proposed rectifier at three input power levels are depicted in Figs. 8(a) and (b). A load resistance of 25 kΩ is selected for the initial study, since it has been the typical load value for many wireless sensors [28], [30]. It can be seen that the proposed rectifier covers the desired six bands for different input power levels of interest. The results agree well at the frequency bands around 550 MHz, 750 MHz, 900 MHz, and 1850 MHz while the measured S_{11} at 2150 MHz and 2450 MHz has shifted to cover a wide bandwidth between 2.2 GHz and 2.4 GHz. This is probably due to the unknown parasitic behavior of the SMD components used in the circuit. The exact values of chip inductors and capacitors are normally a function of frequency. To reduce the influences, products with similar values but different series numbers can be used to replace the components with large values and designed for high frequencies (e.g. L > 20 nH, C > 15 pF, and f > 1 GHz) while multiple identical prototypes can be made to obtain better performance. The RF-to-DC conversion efficiency can be obtained using

$$\eta_{RF-dc} = \frac{P_{DC}}{P_{in}} \quad (7)$$

where P_{DC} is the output DC power, and P_{in} is the input power. The simulated and measured conversion efficiency as a function of frequency is depicted in Fig 9 (a) at three input power levels. At the same power level, it can be seen that the efficiency at lower frequencies (0.5 – 1 GHz) is greater than the efficiency at higher frequencies (1.8 – 2.5 GHz). This is due to the higher loss of diodes and the PCB at higher frequencies. Then, the 25 kΩ load resistance is replaced by other values. The simulated conversion efficiency versus frequency at four different load resistances is shown in Fig. 9 (b). It can be seen that the efficiency over the frequency bands of interest is well maintained for a range of load values from 10 kΩ to 80 kΩ.

The simulated and measured S_{11} as a function of input power level is shown in Fig. 10 at two different frequencies. It can be seen that the rectifier is well matched for input power levels between -30 dBm and -5 dBm at 0.9 GHz while the optimal input power level at 1.85 GHz is from -20 dBm to -5 dBm. The conversion efficiency at these two frequencies as a function of input power level is given in Fig. 11 (a). It can be seen that the maximum efficiency at 0.9 GHz is of around 67% with -5 dBm input while the maximum efficiency at 1.85 GHz is of around 53% with -10 dBm input. The simulated conversion efficiency versus input power level at different load resistances is depicted in Fig.11 (b). It can be seen that, for the load value from 10 kΩ to 80 kΩ, the efficiency is relatively stable for input power level from -30 dBm to -15 dBm, and varies between 40% and 60% for input power level from -15 dBm to -5 dBm. In addition, the multi-tone input signals can enhance the overall conversion

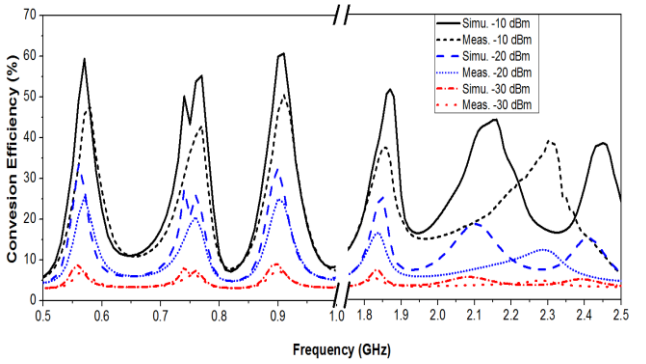

(a)

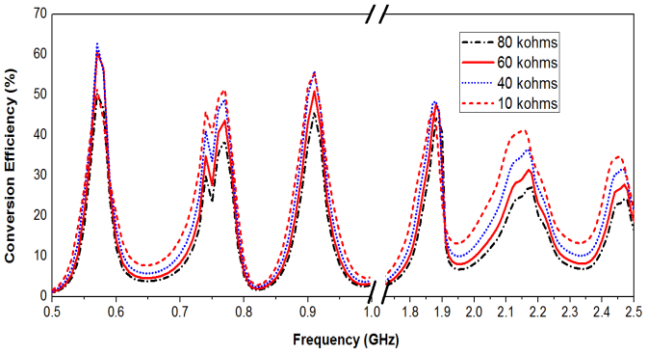

(b)

Fig. 9. (a) The measured and simulated RF-to-DC conversion efficiency of the proposed rectifier at three input power levels for the load resistance of 25 kΩ. (b) The simulated RF-to-DC conversion efficiency of the proposed rectifier at four different load values with the input power level at -10 dBm.

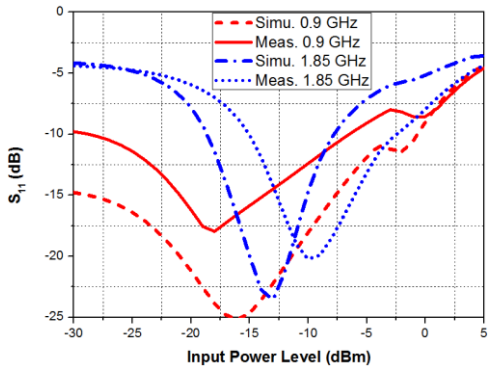

Fig. 10. The measured and simulated S_{11} of the proposed rectifier versus input power level at two frequencies for the load resistance of 25 kΩ.

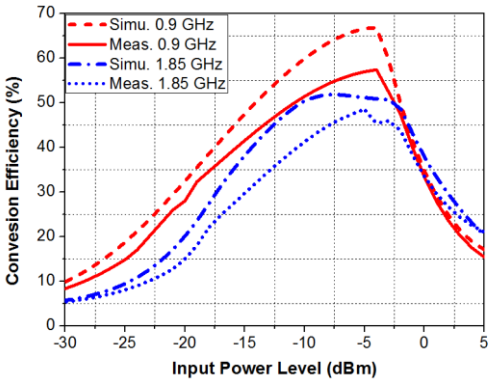

(a)

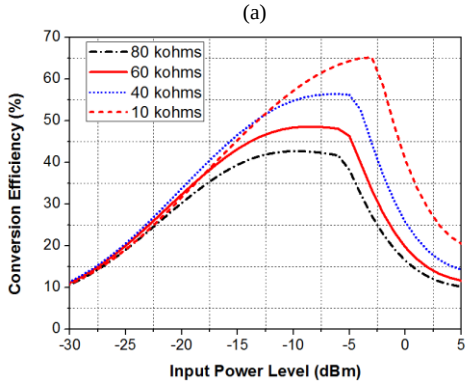

(b)

Fig. 11. (a) The measured and simulated RF-to-DC conversion efficiency of the proposed rectifier versus input power level at two frequencies for the load resistance of 25 kΩ. (b) The simulated RF-to-DC conversion efficiency of the proposed rectifier versus input power level at four different load values. The frequency is 0.9 GHz.

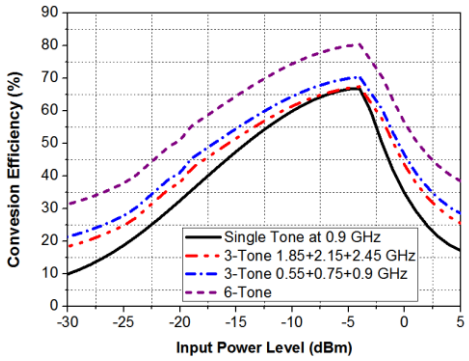

Fig. 12. The simulated RF-to-DC conversion efficiency of the proposed rectifier versus input power level for multi-tone input signals. The load resistance is 25 kΩ.

efficiency of the rectifier which has been demonstrated in [7] and [12]. The simultaneous multi-band input power equals to the sum of RF powers at each tone, which can be expressed as

$$P_m = \sum_{i=1}^{n} P_{fi} \tag{8}$$

where P_m is the multi-band power, P_{fi} is the power at each tone, and n is the number of tones. The conversion efficiency of the simultaneous multi-band input can be obtained by

$$\eta_m = \frac{P_m - P_{Loss}}{P_m} \tag{9}$$

where η_m is the conversion efficiency, and P_{Loss} is the power consumption of the diodes and circuit. Meanwhile, for the combination of separate single band inputs, the conversion efficiency (η_s) can be expressed as the sum of output DC power divided by the total input RF power, as shown in (10)

$$\eta_s = \frac{(P_{f1} - P_{Loss}) + (P_{f2} - P_{Loss}) + \cdots (P_{fn} - P_{Loss})}{P_{f1} + P_{f2} + \cdots P_{fn}} = \frac{P_m - n \times P_{Loss}}{P_m} \tag{10}$$

Therefore, it can be seen that the conversion efficiency of the simultaneous multiband input is greater than the conversion

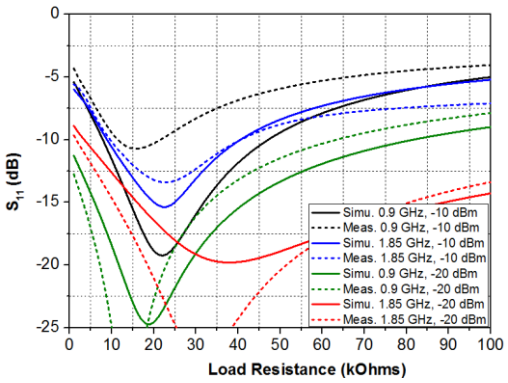

Fig. 13. The simulated and measured S_{11} of the proposed rectifier versus load resistance at two frequencies and two input power levels.

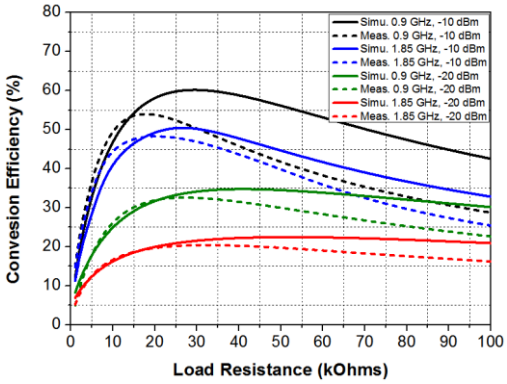

Fig. 14. The simulated and measured RF-to-DC conversion efficiency of the proposed rectifier versus load resistance at two frequencies and two input power levels.

efficiency of the combination of separate single band input powers. The simulated conversion efficiency of the proposed rectifier for single frequency input signal, three-tone input signals and six-tone input signals is depicted in Fig. 12. It can be seen that the maximum conversion efficiency is up to 80% if the rectenna can receive the signals at the six bands simultaneously. In this case, the overall conversion efficiency improvement is about 20%.

To demonstrate that the performance of the rectifier is maintained for a wide range of load resistance, the simulated and measured S_{11} at two frequencies and two input power levels is plotted in Fig. 13 as a function of the load resistance. The frequencies and input power levels in this scenario are 0.9 GHz, 1.85 GHz, -10 dBm, and -20 dBm respectively. It can be seen that, at different frequencies and input power levels, the rectifier works well over a wide range of load impedance from 10 kΩ to 80 kΩ which demonstrates that the influences of the varying load have been reduced. The load-dependent conversion efficiency at two frequencies and two input power levels is depicted in Fig. 14. It can be seen that the efficiency is greater than 50% (at 0.9 GHz, -10 dBm input) and 40% (at 1.85 GHz, -10 dBm input) respectively for the load resistance between 10 kΩ and 75 kΩ. The efficiency is greater than 30% (at 0.9 GHz, -20 dBm input) and 20% (at 1.85 GHz, -20 dBm input) for a load range from 15 kΩ to 90 kΩ. It is demonstrated that the performance of the rectifier is indeed maintained for a wide range of load resistance which is very significant in many real applications.

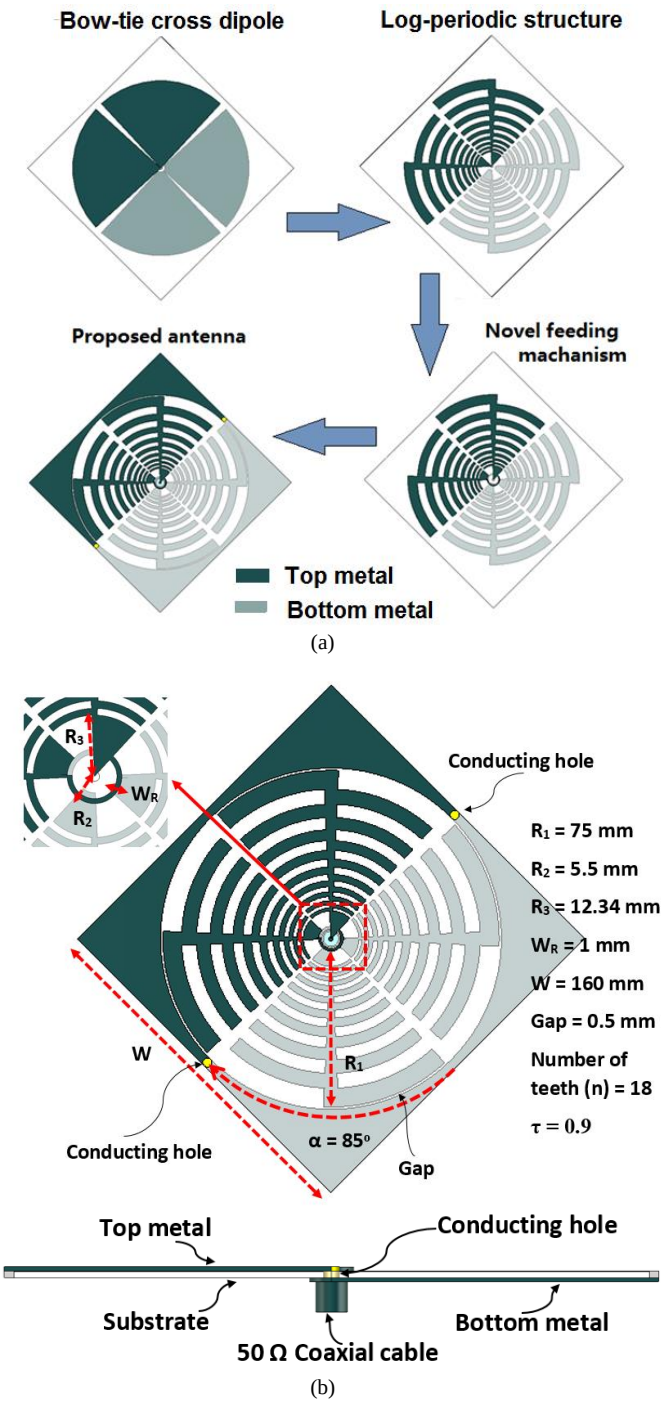

Fig. 15. (a) The evolution of the design; A bow-tie shape cross dipole is modified to a self-complementary log-periodic cross dipole with a novel feeding structure and annular ring structure. (b) The proposed antenna with the optimized dimensions in two views.

III. BROADBAND DUAL CP RECEIVING ANTENNA DESIGN

A bow-tie shape planar cross dipole antenna is proposed as the starting point of the receiving antenna design due to its wide bandwidth, bidirectional radiation pattern, and dual LP characteristics. The proposed antenna is made on an FR4

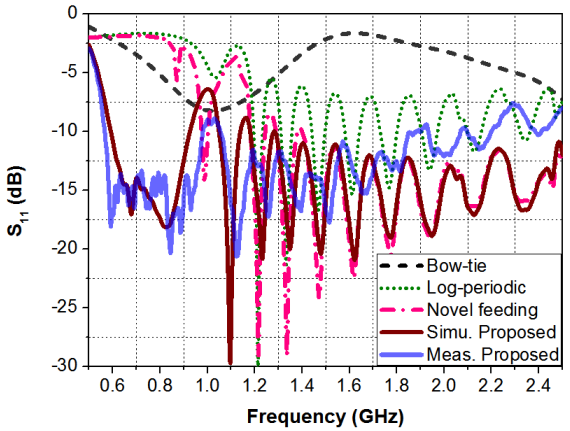

Fig. 16. The simulated S_{11} of the three different antennas and the simulated and measured S_{11} of the proposed antenna.

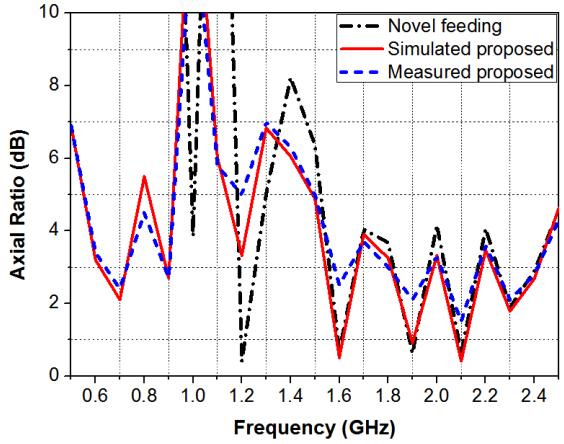

Fig. 17. The simulated axial ratio of the two antennas and the measured axial ratio of the proposed antenna.

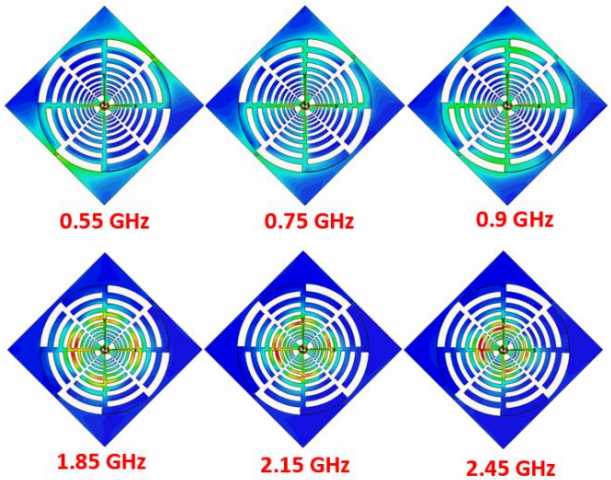

Fig. 18. The simulated current distribution at the frequencies of interest.

substrate with relative permittivity of 4.4 and a thickness of 1.6 mm. The size of the PCB is selected as 160 × 160 mm^2 which equals to $0.29\lambda_0 \times 0.29\lambda_0$ at 550 MHz. The radius and angle of the bowtie shape are selected as 75 mm and 85^o respectively. As shown in Fig. 15(a), two pairs of bow-tie dipoles are produced on both sides of the PCB and orthogonal to each other. The inner conductor of the 50 Ω coaxial cable is fed to

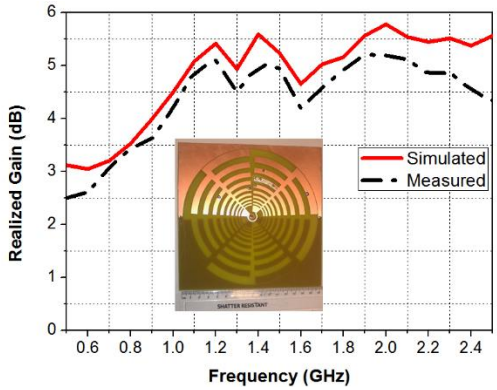

Fig. 19. The simulated and measured realized gains of the antenna. The fabricated prototype antenna is shown as well.

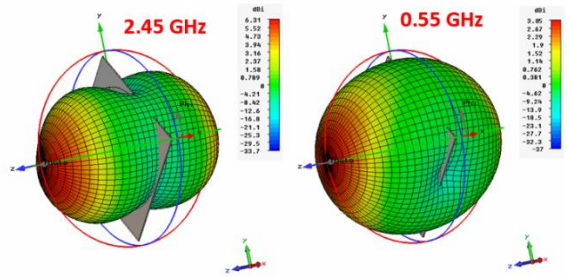

Fig. 20. The simulated 3D radiation patterns at two frequencies.

the top metal of the antenna while the outer conductor is connected to the bottom metal. The simulated S_{11} of the reference bow-tie cross dipole antenna is depicted in Fig. 16. It can be seen that the proposed bow-tie cross dipole resonates at 1 GHz with a wide bandwidth (400 MHz) but the impedance matching performance is not very good (S_{11} > -8 dB). In order to cover a broader bandwidth at higher frequencies (up to 2.5 GHz), the bow-tie cross dipole is modified to a frequency-independent log-periodic cross dipole, as shown in Fig. 15 (a). The number of teeth (n) is selected as 18 and the spacing factor (τ) is chosen as 0.9. From the theory [24], the radius of the nth teeth (R_n) is obtained by using the radius of the (n-1)th teeth (R_{n-1}) multiplied by the spacing factor, as given in (11).

$$R_n = \tau\, R_{n-1} \tag{11}$$

The lowest resonate frequency of the self-complementary log-periodic antenna is normally determined by the radius of the outermost teeth, which is approximately $\lambda_0/4$ in length. Thus, as shown in Fig. 16, the cut-off frequency of the proposed log-periodic cross dipole (R_1 = 75 mm) is around 1 GHz while the active region is between 1 GHz and 2.5 GHz. But, the average level of the simulated S_{11} is around -7.5 dB which means the impedance is not well matched.

In order to improve the performance of the antenna, a novel feeding structure used in [25] which can produce the dual CP radiation field and improve the performance of a conventional cross dipole is employed. As shown in Fig. 15 (a), the pair of dipole is linked by a printed vacant-quarter ring structure in order to generate a 90-degree phase delay and produce the right hand circular polarization (RHCP) radiation field at the front side of the antenna and left hand circular polarization (LHCP)

radiation field at the back side. The simulated S_{11} and axial ratio of the antenna using the novel feeding mechanism are depicted in Figs. 16 and 17 respectively. It can be seen that the matching performance has been improved by using this novel feeding technique. The average level of S_{11} over the bandwidth has been improved from -7.5 dB to -12 dB. In addition, the CP bandwidths of the proposed antenna for axial ratio (AR) less than 3 dB are 1.55 – 1.65 GHz, 1.85 – 1.95 GHz, 2.05 – 2.15 GHz, and 2.25 – 2.4 GHz. The value of AR over 1.6 – 2.5 GHz is lower than 5 dB.

To cover the frequency bands below 1 GHz, an annular ring structure is produced on the PCB with a gap of 0.5 mm to the outermost edge of the antenna. The annular ring is divided in half and printed on both sides of the PCB and electrically connected using two conducting holes as shown in Fig. 15 (b). The complete ring is coupled to the edge of the antenna and becomes a radiator at the lower frequencies [26]. The surface current distribution at the frequencies of interest is shown in Fig. 18. It can be seen that the current flows through the ring structure and the outer teeth of the antenna when the frequency is below 1 GHz which verifies the proposed idea.

The final design of the proposed antenna is shown in Fig. 15 (b) with the optimized dimensions. The simulated and measured S_{11} and axial ratio of the proposed antenna are depicted in Figs. 16 and 17. It can be seen that the results agree reasonably well and an additional band from 550 MHz to 950 MHz is created by adding this ring structure. The CP bandwidth also covers the lower frequencies (0.65 – 0.75 GHz, and 0.9 GHz). Since the sizes of the PCB and the self-complementary log-periodic structure are fixed, the only parameter influences the performance is the gap between the antenna and the annular ring. For a range of value from 0.3 to 1 mm, the effects on the performance are relatively small thus the parametric study is not shown here. The simulated and measured realized gains of the antenna are depicted in Fig. 19. The simulated 3D radiation patterns of the antenna at 550 MHz and 2.45 GHz are shown in Fig. 20. It is shown that the proposed antenna covers the desired frequencies and has dual CP characteristics for most of the frequencies (except 0.55 GHz and 2.45 GHz), and it also has a bidirectional radiation pattern and a compact size. The half power beam-width of the antenna is 120° at 0.55 GHz, 106.3° at 0.75 GHz, 102° at 0.9 GHz, 83.6° at 1.85 GHz, 80.4° at 2.15 GHz and 82.2° at 2.45 GHz respectively.

IV. RECTENNA MEASUREMENT

Having optimized the rectenna, the proposed six-band dual CP rectenna was fabricated. The performance of the rectenna was directly evaluated in reality including the indoor and outdoor environments. A typical office at the University of Liverpool was selected to evaluate the rectenna as an indoor ambient environment. The office has a floor height of 3 meters and an area of 30 m^2 approximately. A public square at the city center of Liverpool was chosen to evaluate the rectenna as an outdoor ambient environment. The square is not in the line-of-sight (LOS) of any high power RF sources such as DTV towers and mobile base stations.

First of all, the proposed broadband dual CP receiving antenna was connected to a portable spectrum analyzer to receive ambient signals. The received ambient signal levels as a function of frequency are depicted in Figs. 21 (a) and (b) for indoor and outdoor scenarios. It can be seen that the DTV signals at the band around 550 MHz cannot be observed in this scenario. For cellular mobile bands, the signal level in outdoor measurement was about -35 to -25 dBm while the level at the indoor environment was lower, from -45 to -35 dBm. In addition, due to the limits of the Wi-Fi router distribution, the received Wi-Fi signals were only available at low levels around -37 dBm at the indoor environment.

Using the same approach as we have proposed in [13], the total received power over the bandwidth was determined by using a wideband power sensor and the average total power was obtained by recording the power as a function of time. It is found that the average total received power in the frequency bands of interest was around -11.4 dBm in outdoor scenario and -13.6 dBm in indoor scenario respectively.

Secondly, the proposed rectifier was connected to the antenna and the output voltage was measured by using a voltage meter. As shown in Figs. 21 (a) and (b), the measured output voltage was around 600 mV in outdoor scenario with a load value of 15 kΩ while the voltage was about 400 mV at the indoor environment with a load value of 30 kΩ. The corresponding harvested DC power in outdoor and indoor environment was around 24 μW and 5.6 μW respectively. To demonstrate that the performance of the rectenna is maintained for a wide range of load impedance, the output DC voltage was also measured by changing the load resistance from 5 kΩ to 100 kΩ. The measured maximum harvested DC powers in indoor and outdoor ambient environment were 26 μW (load resistance: 36 kΩ) and 8 μW (load resistance: 45 kΩ) respectively. The overall conversion efficiency was calculated as the fraction of the output power and the average total received power in the band as we have obtained in the previous steps, which can be expressed as

$$\eta_{overall} = \frac{P_{DC}}{P_{ave}} = \frac{V_{DC}^2}{R_L P_{ave}} \quad (12)$$

where P_{DC} is the output power, P_{ave} is the average total received power in the band (outdoor: -11.4 dBm, indoor: -13.6 dBm), V_{DC} is the output voltage, and R_L is the load. In order to improve the accuracy of the results, the experiment was conducted in multiple times and the overall conversion efficiency is depicted in Fig. 22 with an error bar. It can be seen that for a wide range of load between 10 kΩ and 75 kΩ, the measured overall conversion efficiency is up to 26% for outdoor environment and 13% for indoor environment. At such a low power level (e.g. -30 dBm), the measured efficiency of the proposed rectenna is much higher than the conversion efficiency of many conventional single band rectennas (e.g. < 5%). Also, the same advantage could be obtained if the input power level becomes higher (up to -5 dBm). The simulated maximum conversion efficiency of the rectenna at a single frequency input is about 67% (at -5 dBm input) while the efficiency can go up to 80% for simultaneous multi-band input signals.

TABLE II
COMPARISON OF THE PROPOSED RECTENNA AND RELATED DESIGNS

Ref. (year)	Frequency (GHz)	Random polarization receiving capability	Input power level of interest (dBm)	Maximum RF-dc conversion efficiency at a single frequency (%)	Maximum conversion efficiency at multi-tone input (%)	Optimal load range with performance is maintained (kΩ)	Measured/simulated harvested DC power at the outdoor ambient input power level (-15 dBm)
[7] (2013)	Dual-band 1.8, 2.2	NA*	-30 to -5	55 at -5 dBm	55	5	28 μW (measured)
[8] (2013)	Four-band 0.9 , 1.75, 2.15, 2.45	NA*	-15 to 0	60 at 0 dBm	NR*	NR*	13 μW (measured)
[9] (2013)	Dual-band 0.915, 2.45	NA*	-15 to 0	50 at 0 dBm	50	2.2	17 μW (measured)
[12] (2015)	Four-band 0.9, 1.8, 2.1, 2.4	Dual LP	-25 to 0	65 at 0 dBm	84	11	70 μW (measured)
[13] (2015)	Broad-band 1.8 – 2.5	Dual LP	-35 to -10	70 at 0 dBm	NR*	14.7	53 μW (measured)
[15] (2014)	Dual-band 0.915, 2.45	NA*	-30 to 0	70 at 0 dBm	NR*	0.5 – 3	26 μW (simulated)
[16] (2014)	Single-band 2.45	NA*	13 to 20	80 at 13 dBm	NA*	0.1 – 5	NA*
[31] 2013	Four-band 0.55, 0.9, 1.85, 2.15	NA*	-29 to -10	40 at -12 dBm	NA*	NR*	38 μW (measured)
This work (2016)	**Six-band 0.55, 0.75, 0.9, 1.85, 2.15, 2.45**	**Dual CP**	**-30 to -5**	**67 at -5 dBm**	**80**	**10 – 75**	**96 μW (measured)**

*NA: Not Available. NR: Not Reported

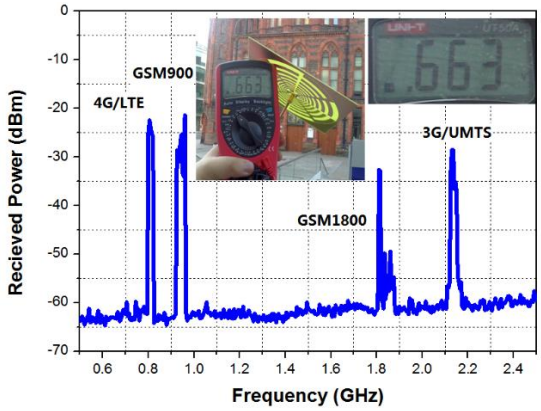

(a)

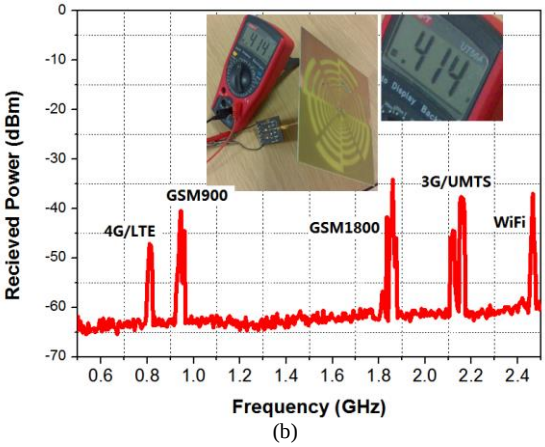

(b)

Fig. 21. The measured received power versus frequency and the measured output voltage of the proposed rectenna in (a) Outdoor ambient environment. (b) Indoor ambient environment.

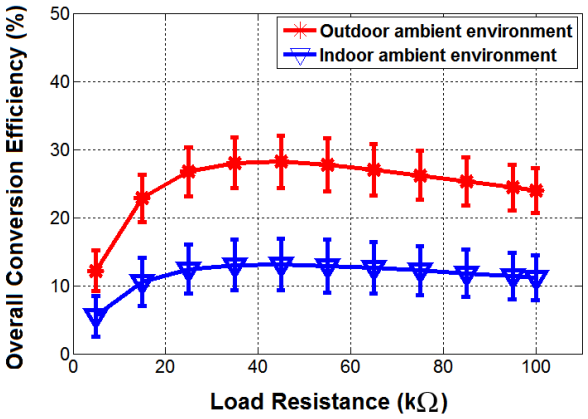

Fig. 22. The measured overall RF-to-DC conversion efficiency with an error bar for indoor and outdoor scenarios.

A comparison between our rectenna design and some recent rectenna and rectifier designs is given in Table II. It can be seen that our design seems to be the only one which can harvest energy from the ambient signals at six frequency bands simultaneously. If we compare their harvested DC powers at a typical outdoor ambient RF power level (-15 dBm), the measured/simulated output powers from their designs are much smaller than ours. Although the measured results have shown that the proposed rectenna is only effective at five frequency bands, the measured harvested DC power of our device is still the highest. In addition, our design has a random polarization receiving capability which can improve the overall performance. Most of the published designs are optimized to a fixed load and the conversion efficiency is heavily dependent on the varying conditions. Our device has a stable performance for a wide range of load, from 10 kΩ to 75 kΩ, which covers the equivalent load impedance of many wireless sensors and

monitors [27]–[30]. The proposed rectenna is better than the other published designs in terms of the overall performance thus is a very good candidate for RF energy harvesting in many real world applications.

V. CONCLUSION

A novel six-band dual CP rectenna has been proposed using an improved impedance matching technique. The newly designed matching network can maintain the excellent performance of the rectenna in various conditions such as multiple frequency bands, different input power levels and a wide range of load. This is very important for wireless energy harvesting. A broadband dual CP receiving antenna has been proposed. A novel feeding structure has been used to generate the dual CP radiation field and improve the performance while an annular ring structure has been proposed to cover the lower frequency bands. The simulated maximum conversion efficiency at a single frequency has been obtained at 67% with -5 dBm input at 0.9 GHz. The optimal load range in which the performance of the rectenna is maintained is from 10 kΩ to 75 kΩ for the load impedance. The measured results have shown that the overall conversion efficiency is about 26% and 13% in a typical outdoor and indoor ambient environment. The proposed rectenna is better than the other published designs in terms of the overall conversion efficiency as well as the coverage of frequency band and load range. Considering the outstanding performance of the rectenna with different conditions, the proposed design is very suitable for many real world low power devices and can therefore be applied in many battery-free wireless applications.

ACKNOWLEDGMENT

The authors appreciate the constructive feedback from the anonymous reviewers of this paper. The authors would also like to thank Simon Hau from Murata Ltd. for the donation of SMD circuit components.

REFERENCES

[1] S. Kim, R. Vyas, J. Bito, K. Niotaki, A. Collado, A. Georgiadis, and M. M. Tentzeris, "Ambient rf energy-harvesting technologies for self-sustainable standalone wireless sensor platforms," *Proc. IEEE*, vol. 102, no. 11, pp. 1649–1666, Nov. 2014.

[2] W. C. Brown, ''The history of power transmission by radio waves,'' *IEEE Trans. Microw. Theory Tech*., vol. 32, no. 9, pp. 1230–1242, Sep. 1984.

[3] Y. J. Ren and K. Chang, "5.8-GHz circularly polarized dual-diode rectenna and rectenna array for microwave power transmission," *IEEE Trans. Microw. Theory Tech*., vol. 54, no. 4, pp. 1495–1502, 2006.

[4] B. Strassner and K. Chang, "5.8-GHz circularly polarized dual rhombic-loop travelling-wave rectifying antenna for low power-density wireless power transmission applications," *IEEE Trans. Microw. Theory Tech*., vol. 51, no. 5, May 2003.

[5] J. O. McSpadden, F. Lu, and K. Chang, "Design and experiments of a high conversion efficiency 5.8-GHz rectenna," *IEEE Trans. Microw. Theory Tech*., vol. 46, no. 12, pp. 2053–2060, Dec. 1998.

[6] B. Strassner and K. Chang, "Highly efficient -band circularly polarized rectifying antenna array for wireless microwave power transmission," *IEEE Trans. Antennas Propag*., vol. 51, no. 6, pp. 1347–1356, Jun. 2003.

[7] H. Sun, Y.-x. Guo, M. He and Z. Zhong, "A dual-band rectenna using broadband Yagi antenna array for ambient RF power harvesting," *IEEE Antennas and Wireless Propa. Lett.*, vol. 12, pp. 918–921, 2013.

[8] D. Masotti, A. Costanzo, M. D. Prete and V. Rizzoli, "Genetic-based design of a tetra-band high-efficiency radio-frequency energy system,"*Microw. Antennas Propag.*, vol. 7, no. 15, pp. 1254–1263, Jun. 2013.

[9] K. Niotaki, S. Kim, S. Jeong, A. Collado, A. Georgiadis, and M. Tentzeris, "A compact dual-band rectenna using slot-loaded dual band folded dipole antenna," *IEEE Antennas and Wireless Propa. Lett.* vol. 12, pp. 1634–1637, 2013.

[10] R. Scheeler, S. Korhummel and Z. Popovic, "A dual-frequency ultralow-power efficient 0.5-g rectenna," *IEEE Microwave Mag*., vol. 15, no. 1, pp. 109–114, Jan. 2014.

[11] J. A. Hagerty, F. B. Helmbrecht, W. H. McCalpin, R. Zane and Z. B. Popovic, "Recycling ambient microwave energy with broad-Band rectenna Arrays," *IEEE Trans. Microw. Theory Tech*., vol. 52, no. 3, pp. 1014–1024, Mar. 2004.

[12] V. Kuhn, C. Lahuec, F. Seguin, and C. Person, "A multi-band stacked RF energy harvester with rf-to-dc efficiency up to 84%," *IEEE Trans. Microw. Theory Tech*., vol. 63, no. 5, pp. 1768–1778, May 2015.

[13] C. Song, Y. Huang, J. Zhou, J. Zhang, S. Yuan and P. Carter, "A high-efficiency broadband rectenna for ambient wireless energy harvesting," *IEEE Trans. Antennas Propag*., vol. 63, no. 8, pp. 3486–3495, May 2015.

[14] Y. Han, O. Leitermann, D. A. Jackson, J. M. Rivas, and D. J. Perreault, "Resistance compression networks for radio-frequency power conversion," *IEEE Trans. Power Electron*., vol. 22, no. 1, pp. 41–53, Jan. 2007

[15] K. Niotaki, A. Georgiadis, A. Collado, and J. S. Vardakas, "Dual-band resistance compression networks for improved rectifier performance," *IEEE Trans. Microw. Theory Tech.*, vol. 62, no. 12, pp. 3512–3521, Nov. 2015.

[16] Y. Huang, N. Shinohara, and T. Mitani, "A constant efficiency of rectifying circuit in an extremely wide load range," *IEEE Trans. Microw. Theory Tech*., vol. 62, no. 4, pp. 986–993, Apr. 2014.

[17] J. F. Xu, W. Tai, and D. S. Ricketts, "A transmission line based resistance compression network (TRCN) for microwave applications," in *2013 IEEE MTT-S Int. Microw. Symp.* Dig., Seattle, WA, USA, pp.1–3.

[18] W. Inam, K. K. Afridi, and D. J. Perreault, "High efficiency resonant dc/dc converter utilizing a resistance compression network," *IEEE Trans. Power Electron*., vol. 29, no. 8, pp. 4126–4135, Aug. 2014.

[19] T. Paing, J. Shin, R. Zane, and Z. Popovic, "Resistor emulation approach to low-power RF energy harvesting," *IEEE Trans. Power Electron*., vol. 23, no. 3, pp. 1494–1501, 2008.

[20] Z. Safarian and H. Hashemi, "Wirelessly powered passive systems with dynamic energy storage mechanism," *IEEE Trans. Microw. Theory Tech.*, vol. 62, no. 4, pp. 1012–1021, Apr. 2014.

[21] B. Merabet, F. Costa, H. Takhedmit, C. Vollaire, B. Allard, L. Cirio, and O. Picon, "A 2.45-GHz localized elements rectenna," in *Proc. 3rd IEEE Int. Symp. Microw., Antenna, Propag. EMC Technol. Wireless Commun.*, Oct. 2009, pp. 419–422.

[22] C. R. Valenta and G. D. Durgin, "Harvesting wireless power: Survey of energy-harvester conversion efficiency in far-field, wireless power transfer systems," *IEEE Microw. Mag*., vol. 15, no. 4, pp. 108–120, May. 2014.

[23] *Surface Mount Mixer and Detector Schottky Diodes, Data Sheet*. Skyworks Solutions, Inc., Woburn, MA, USA, 2013.

[24] R. Duhamel and D. Isbell, "Broadband logarithmically periodic antenna structures," *IRE Int. Convention Record*, vol. 5, pp. 119–128, Mar. 1957.

[25] S. X. Ta , H. Choo , I. Park and R. W. Ziolkowski, "Multi-band, wide beam, circularly polarized, cross, asymmetrically barbed dipole antennas for GPS applications" *IEEE Trans. Antennas Propag*., vol. 61, no. 11, pp. 5771-5775, 2013.

[26] R. Sammeta and D. S. Filipovic, "Quasi frequency-independent increased bandwidth planar log-periodic antenna," *IEEE Trans. Antennas Propag.*, vol. 62, no. 4, pp. 1937–1944, Apr. 2014.

[27] J. Van Rethy et al., "A low-power and low-voltage BBPLL-based sensor interface in 130 nm CMOS for wireless sensor networks," *in Design, Autom. Test Eur. Conf. Exhibit*., Mar. 2013, pp. 1431–1435.

[28] S. W. Chen, M. H. Chang, W. C. Hsieh, and W. Hwang, "Fully on-chip temperature, process, and voltage sensors," *in Proc. IEEE Int. Circuits Syst. Symp*., 2010, pp. 897–900.

[29] A. Dolgov, R. Zane, and Z. Popovic, "Power management system for online low power RF energy harvesting optimization," *IEEE Trans. Circuits Syst. I, Reg. Papers*, vol. 57, pp. 1802–1811, Jul. 2010.
[30] E.G. Bakhoum, "High-sensitivity miniature smoke detector," *IEEE Sensors Journal*, vol. 12, no. 10, pp. 3031–3035, Jul. 2012.
[31] M. Piñuela, P. D. Mitcheson, and S. Lucyszyn, "Ambient RF energy harvesting in urban and semi-urban environments," *IEEE Trans. Microw. Theory Tech.*, vol. 61, no. 7, pp. 2715–2726, Jul. 2013.

Chaoyun Song (S'16) was born in Gansu, China, in 1990. He received the B.Eng degree (Hons) in telecommunication engineering from Xi'an Jiao Tong Liverpool University, Suzhou, China, in 2012 and the M.Sc. degree with distinction in microelectronics and telecommunication from the University of Liverpool, Liverpool, United Kingdom, in 2013. He is currently working toward the Ph.D. degree in wireless communications and RF engineering at the University of Liverpool, UK.

He has been a regular reviewer of 2 IEEE Transactions. His research interests include rectifying-antenna, circular polarization antenna, power management circuit, wireless power transfer and energy harvesting, and wearable antennas.

Yi Huang (S'91–M'96–SM'06) received the B.Sc. degree in physics from Wuhan University, Wuhan, China, in 1984, the M.Sc. (Eng.) degree in microwave engineering from NRIET, Nanjing, China, in1987, and the Dr. Phil. degree in communications from the University of Oxford, Oxford, U.K., in 1994.

His experience includes three years spent with NRIET, as a Radar Engineer, and various periods with the Universities of Birmingham, Oxford, and Essex, in the U.K., as a Member of Research Staff. He was a Research Fellow with British Telecom Labs in 1994, and, then, joined the Department of Electrical Engineering and Electronics, the University of Liverpool, Liverpool, U.K., as a Faculty Member in 1995, where he is currently a Full Professor in Wireless Engineering, the Head of High Frequency Engineering Research Group, M.Sc. Programme Director, and Deputy Head of Department. He has published more than 200 refereed papers in leading international journals and conference proceedings, and is the principal Author of the popular book "Antennas: From Theory to Practice" (New York, NY, USA: Wiley, 2008). He has received many research grants from research councils, government agencies, charity, EU, and industry, acted as a consultant to various companies, and served on a number of national and international technical committees. From past 25 years, his research interests include wireless communications, applied electromagnetics, radar, and antennas.

Prof. Huang has been an Editor, Associate Editor, or Guest Editor of four of international journals. He has been a keynote/invited speaker and organizer of many conferences and workshops (e.g., IEEE iWAT 2010, WiCom 2006, 2010, and LAPC2012). He is currently the Editor-in-Chief of Wireless Engineering and Technology, a U.K. National Rep of European COST-IC1102, an Executive Committee Member of the IET Electromagnetics PN, and a Fellow of IET, U.K.

Paul Carter received the B.Sc. degree (Hons.) in physics from the University of Manchester, U.K., in 1987, the M.Sc. degree (Eng.) in microelectronic systems and telecommunications, in 1988, and the Ph.D. degree in electrical engineering and electronics, in 1992 both from the University of Liverpool, U.K.

He is the President and CEO of Global Wireless Solutions, Inc. (GWS), Dulles, VA, USA, a leading independent benchmarking solution vendor for the wireless industry. With more than 25 years of experience in the cellular network industry, he founded Global Wireless Solutions to provide operators with access to in-depth, accurate network benchmarking, analysis, and testing. Prior to GWS, he directed business development and CDMA engineering efforts for LLC, the world's largest independent wireless engineering company.

Jiafeng Zhou received the B.Sc. degree in Radio Physics from Nanjing University, Nanjing, China, in 1997, and the Ph.D. degree from the University of Birmingham, Birmingham, U.K., in 2004. His doctoral research concerned high-temperature superconductor microwave filters.

From July 1997, for two and a half years he was with the National Meteorological Satellite Centre of China, Beijing, China, where he was involved with the development of communication systems for Chinese geostationary meteorological satellites. From August 2004 to April 2006, he was a Research Fellow with the University of Birmingham, where his research concerned phased arrays for reflector observing systems. Then he moved to the Department of Electronic and Electrical Engineering, University of Bristol, Bristol, U.K until August 2013. His research in Bristol was on the development of highly efficient and linear amplifiers. He is now with the Department of Electrical Engineering and Electronics, University of Liverpool, Liverpool, UK. His current research interests include microwave power amplifiers, filters, electromagnetic energy harvesting and wireless power transfer.

Sheng Yuan was born in Shanghai, China, in 1990. He received the B.Eng degree (first class) in microelectronics and telecommunication engineering from the University of Liverpool, Liverpool, United Kingdom, in 2012. He is currently working toward the Ph.D. degree in wireless communications and RF engineering at the University of Liverpool, UK.

His research interests include indoor navigation and communication, magnetic field energy harvesting, wireless power transfer, and RFID.

Qian Xu received the B.Eng. and M.Eng. degrees from the Department of Electronics and Information, Northwestern Polytechnical University, Xi'an, China, in 2007 and 2010, and received the PhD degree in electrical engineering from the University of Liverpool, U.K, in 2016.

He worked as a RF engineer in Nanjing, China in 2011 and an Application Engineer in CST, Shanghai, China in 2012. His research interests include statistical electromagnetics, computational electromagnetics, reverberation chamber and anechoic chamber.

Muayad Kod received the B.Sc. and M.Sc. degrees from the Department of Electronics and Communications, Al-Nahrain University, Baghdad, Iraq, in 2002 and 2005 respectively. In 2005, he worked as an OMC Engineer in Orascom Telecom/Iraqna (It's known now as Global Telecom Holding). In 2007, he joined Asiacell for telecommunication as RF engineer in the middle region of Iraq. In August 2008, he moved to Omnnea for Wireless Telecommunications as RF engineering team leader. Since October 2009, he worked as an assistant lecturer in the department of Electrical Engineering and Electronics, University of Kerbala, Iraq.

He is currently working toward the Ph.D. degree at the department of Electrical Engineering and Electronics, University of Liverpool, the UK. His current research interests include wireless power transfer and telemetry to implantable medical devices, wearable and implantable antennas, RFID and energy harvesting.